

1 Constraint-based metabolic control analysis for 2 rational strain engineering

3
4 Sophia Tsouka^{1,*}, Meric Ataman^{1,2,*}, Tuure Hameri¹, Ljubisa Miskovic¹, Vassily
5 Hatzimanikatis^{1,†}

6

7 * equally contributing authors

8 ¹Laboratory of Computational Systems Biology (LCSB), EPFL, CH-1015 Lausanne, Switzerland.

9 ² current address: Computational and Systems Biology, Biozentrum University of Basel, Klingelbergstrasse 50-
10 70, 4056, Basel, Switzerland

11 [†] Corresponding author:

12 Vassily Hatzimanikatis,

13 Laboratory of Computational Systems Biotechnology (LCSB), École Polytechnique Fédérale de Lausanne (EPFL),
14 CH-1015 Lausanne, Switzerland

15 **Email:** vassily.hatzimanikatis@epfl.ch, **Phone:** +41 (0)21 693 98 70, **Fax:** +41 (0)21 693 98 75

16

17 **Abstract**

18 The advancements in genome editing techniques over the past years have rekindled interest
19 in rational metabolic engineering strategies. While Metabolic Control Analysis (MCA) is a well-
20 established method for quantifying the effects of metabolic engineering interventions on
21 flows in metabolic networks and metabolic concentrations, it fails to account for the
22 physiological limitations of the cellular environment and metabolic engineering design
23 constraints. We report here a constraint-based framework based on MCA, Network Response
24 Analysis (NRA), for the rational genetic strain design that incorporates biologically relevant
25 constraints, as well as genome editing restrictions. The NRA core constraints being similar to
26 the ones of Flux Balance Analysis, allow it to be used for a wide range of optimization criteria
27 and with various physiological constraints. We show how the parametrization and
28 introduction of biological constraints enhance the NRA formulation compared to the classical
29 MCA approach, and we demonstrate its features and its ability to generate multiple
30 alternative optimal strategies given several user-defined boundaries and objectives. In
31 summary, NRA is a sophisticated alternative to classical MCA for rational metabolic

32 engineering that accommodates the incorporation of physiological data at metabolic flux,
33 metabolite concentration, and enzyme expression levels.

34

35

36 Introduction

37 Recent improvements in genome editing techniques have paved the way for more
38 sophisticated and performant metabolic engineering designs for achieving desired
39 physiological states of host organisms. Two approaches for reaching the targeted states exist:
40 (i) integrating heterologous pathways to disruptively overcome native control patterns, and
41 (ii) modifying the endogenous regulatory architecture by removal of the existing control loops
42 (Bailey, 1991). The former method can be rather arduous because it requires testing if the
43 integration of DNA fragments into the original genome sequence perturbs cellular regulation
44 in the desired fashion. The latter technique demands knowledge about cellular control so that
45 the DNA sequence can be modified effectively and without unwanted side effects.

46 Mathematical models are nowadays becoming an indispensable part of strain design.
47 Available gene-protein-reaction associations of various organisms provide invaluable
48 information about cellular metabolism and enable the elaboration of these models. The
49 models can be studied computationally to interrogate and analyze cellular behavior and
50 derive metabolic engineering strategies for improved cellular performance (Gombert and
51 Nielsen, 2000). Strain design requires the identification and engineering of pathways toward
52 the production of desired compounds (Hadadi and Hatzimanikatis, 2015), and mathematical
53 models can provide an invaluable insight in the process of selection of deletions, insertions,
54 and up- and down-regulation of genes encoding for metabolic enzymes. Reviews of the most
55 prominent computational tools and workflows for the strain design are provided elsewhere
56 (Costa et al., 2016; Long et al., 2015; Wang et al., 2017).

57 Metabolic control analysis (MCA) is a mathematical formalism that uses models to quantify
58 the distribution of control over metabolic states in a network such as fluxes and
59 concentrations (Kacser et al., 1995). In MCA, Control Coefficients (CCs) quantify how a given
60 metabolic flux or metabolite concentration would respond to perturbations of the system
61 parameters. This information is used in traditional rational metabolic design to identify the
62 rate-limiting steps of the network and select potential targets for engineering. Strain
63 engineering typically requires a holistic approach where one simultaneously analyzes the
64 effects of genetic manipulations on specific productivity of desired molecules, maximum
65 achievable yield, energetic and redox requirements, etc. Simultaneous analysis of these
66 effects is a cumbersome task using classical MCA tools, especially if the design requires

67 multiple genetic alterations. Moreover, MCA does not allow including explicitly any form of
68 physiological or design constraints, which can lead to unrealistic predictions.

69 We present here Network Response Analysis (NRA), a constraint-based workflow that aims
70 to tackle these obstacles. NRA utilizes populations of CCs to consistently derive metabolic
71 engineering strategies and trace the effects of multiple parameter perturbations. The
72 advantage of this method is that physiologically relevant bounds and constraints can be
73 imposed to the system, as opposed to the classical MCA. NRA is inspired by the work by
74 Hatzimanikatis et al. (1996a); (1996b) who proposed a Mixed Integer Linear Programming
75 (MILP) formulation for querying cellular responses upon enzymatic perturbations that uses
76 MCA-based flux and concentration CCs. Therein, the authors applied their formulation on
77 simple linear and branched pathways to propose metabolic engineering strategies. Here, we
78 extend this formulation to allow for studying larger scale metabolic systems with guaranteed
79 thermodynamic feasibility.

80 To illustrate how NRA can be used to efficiently analyze, enumerate, and propose alternative
81 metabolic engineering strategies, we used a large-scale thermodynamically-curated,
82 metabolic model of *E. coli* (Hameri et al., 2019c), which describes the central carbon pathways
83 in aerobic growth conditions. Using the stoichiometric model as a scaffold, we employed the
84 ORACLE framework (Andreozzi et al., 2016a; Chakrabarti et al., 2013; Hameri et al., 2019b;
85 Miskovic et al., 2017; Miskovic and Hatzimanikatis, 2010; Soh et al., 2012; Tokic et al., 2020)
86 to generate populations flux and concentration CCs consistent with the experimental
87 observations. We then used the generated CCs to formulate with NRA the design strategies
88 in two case studies (i) improvement of glucose uptake rate, and (ii) maximization of specific
89 productivity rate of pyruvate while preserving a pre-specified yield of pyruvate from glucose.
90 These studies clearly show the potential, flexibility, and ease of use of NRA when realistic,
91 multi-objective requirements for the strain design should be met.

92 **Results and Discussion**

93 **NRA method**

94 The first step of the NRA method is the selection and curation of a metabolic network that
95 captures the physiology of a studied organism (Fig. 1). Then, we calculate the relevant flux
96 and concentration CCs (FCCs and CCCs) that describe the network's responses to parameter

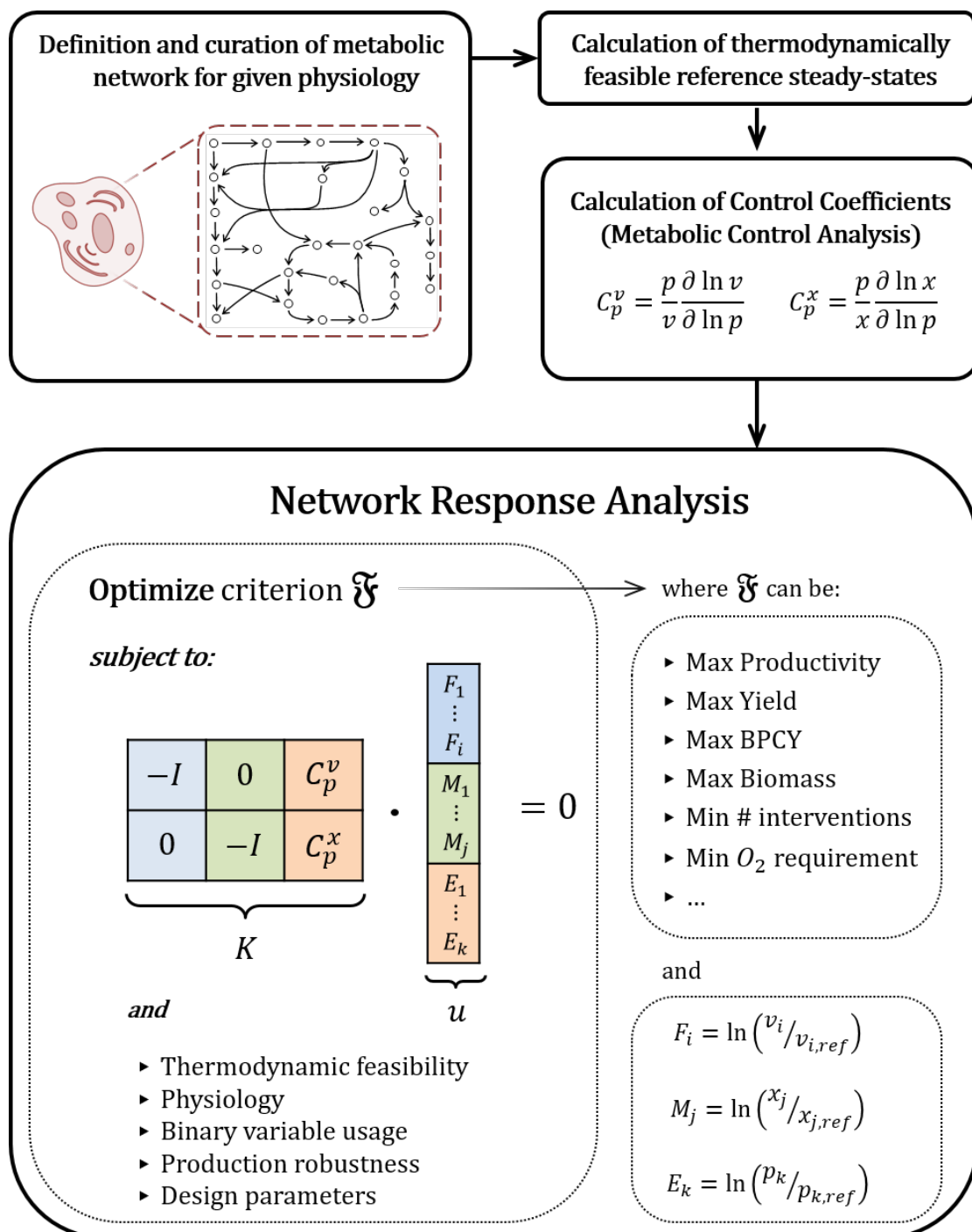
97 perturbations such as modifications of enzymatic activities with the ORACLE framework,
98 which makes use of Monte Carlo sampling (Miskovic and Hatzimanikatis, 2011; Wang et al.,
99 2004). Finally, we use the computed sets of CCs along with the user-defined requirements
100 and additional physiological constraints to construct a constraint-based MILP optimization
101 problem (Fig. 1). The user-defined inputs depend on the studied problem and design
102 limitations, and these typically include the number of desired gene manipulations, minimal
103 allowable specific productivity, minimum allowable yield, etc. From experimental
104 measurements or assumptions on physiology, we can infer physiological constraints such as
105 allowable (or desired) bounds on fluxes and concentrations in the metabolic network.

106 The outcome of the NRA optimization are sets of alternative combinations of genes that
107 should be engineered to improve the cellular performance given the imposed user-defined
108 inputs and physiological constraints. A principal advantage of the MILP formulation is that it
109 allows the user to introduce constraints on metabolic states and additional relevant design
110 constraints to the system, thus simultaneously offering flexibility and tight control over the
111 rational strain design.

112

113 *NRA formulation*

114 The NRA core equations can be expressed in a matrix-vector form (Table 1, Eq. 7) similar to
115 the ones of Flux Balance Analysis (FBA) (Orth et al., 2010) and Thermodynamics-based Flux
116 Analysis (TFA) (Henry et al., 2007; Salvy et al., 2019). NRA accommodates a wide gamut of
117 design objectives, such as the maximization of productivity or product yield (Eqs. 1-2),
118 biomass-product coupled yield (BPCY) (Eq. 3), the maximization of biomass formation (Eq. 4),
119 the minimization of required genome-editing interventions (Eq. 5), and the minimization of
120 oxygen requirements (Eq. 6) (Klamt et al., 2018; Patil et al., 2005; Schneider and Klamt, 2019;
121 Varma et al., 1993). Since we have defined the NRA variables in logarithmic form, we can
122 express the otherwise nonlinear objectives like yield or BPCY in a linear form, rendering the
123 solution of the mathematical problem easier to attain than with formulations such as FBA.



124

125 *Figure 1. The NRA workflow is organized in four main steps. In the first three steps, we formulate the*
 126 *stoichiometry, integrate available experimental data and compute the steady-state*
 127 *thermodynamically feasible fluxes and concentrations, and compute the flux and concentration control*
 128 *coefficients for the studied physiological condition. In the fourth step, metabolic engineering strategies*
 129 *are devised by solving a MILP. Criterion \mathcal{F} and additional constraints can be chosen from a set of*
 130 *metabolic engineering criteria such as the ones provided in Table 1. Variables F_i , M_j and E_k are the*

131 *logarithmic deviations in flux, metabolite concentration and parameter with respect to their respective*
 132 *reference steady states (Eq. 23), and their bounds define the solution space of the optimization*
 133 *problem (Eqs. 8-10). The definition of the other optimization variables and parameters is given in Table*
 134 *2.*

135

136 *Table 1. The NRA mathematical formulation together with a non-exhaustive selection of optimization objectives. The*
 137 *definition of indices, parameters, and variables is provided in Table 2.*

Optimize Criterion \mathcal{F} :

	FBA	NRA
Max productivity	$\max v_{product}$	$\max \tilde{F}_{product}$ (1)
Max yield	$\max \frac{v_{product}}{v_{substrate}}$	$\max \tilde{F}_{product} - \tilde{F}_{substrate}$ (2)
Max BPCY	$\max v_{biomass} * \frac{v_{product}}{v_{substrate}}$	$\max \tilde{F}_{biomass} + \tilde{F}_{product} - \tilde{F}_{substrate}$ (3)
Max biomass	$\max v_{biomass}$	$\max \tilde{F}_{biomass}$ (4)
Min # interventions	—	$\min \sum_{k \in \mathcal{K}} (1 - z_k)$ (5)
Min O_2 requirement	$\min v_{O_2, uptake}$	$\min \tilde{F}_{O_2, uptake}$ (6)

subject to constraints:

	FBA	NRA
Balance (Mass / Response)	$N \cdot v = 0$	$K \cdot u = 0$ $\Leftrightarrow \left\{ \begin{array}{l} F_i - \sum_{k \in \mathcal{K}} (C_{E_k}^{v_i} * E_k) = 0 \\ M_j - \sum_{k \in \mathcal{K}} (C_{E_k}^{x_j} * E_k) = 0 \end{array} \right\}$ (7)
Variable bounds	$lb \leq v_i \leq ub$	$lb_F \leq F_i \leq ub_F$ (8) $lb_M \leq M_j \leq ub_M$ (9) $lb_E \leq E_k \leq ub_E \Leftrightarrow \left\{ \begin{array}{l} 0 \leq E_k^U \leq ub_E \\ 0 \leq E_k^D \leq -lb_E \end{array} \right\}$ (10)
Binary variable usage	—	$E_k^U + E_k^D + \xi * z_k \leq \xi$ (11) $E_k^{UU} + E_k^{DU} \leq 1$ (12) $E_k^U - \xi * E_k^{UU} < 0$ (13) $E_k^D - \xi * E_k^{DU} < 0$ (14)

Thermodynamic feasibility

—	$\Delta_r G'_i < 0 \Leftrightarrow \Delta_r G'^o_i + RT \sum_{m \in \mathcal{M}} \tilde{M}_m^i < 0 \quad (15)$
---	--

and

	<i>FBA</i>	<i>NRA</i>
Production robustness (min productivity)	$v_{product} \geq \alpha_0$	$\tilde{F}_{product} \geq \beta_0 \quad (16)$
Production robustness (min yield)	$\frac{v_{product}}{v_{substrate}} \geq \alpha_1$	$\tilde{F}_{product} - \tilde{F}_{substrate} \geq \beta_1 \quad (17)$
Production robustness (min biomass)	$v_{biomass} \geq \alpha_2$	$\tilde{F}_{biomass} \geq \beta_2 \quad (18)$
Design parameters (max # interventions)	—	$\sum_{k \in \mathcal{K}} (1 - z_k) \leq \beta_3 \quad (19)$
Design parameters (max O_2 requirement)	$v_{O_2, uptake} \leq \alpha_3$	$\tilde{F}_{O_2, uptake} \leq \beta_4 \quad (20)$

where

$$K = \begin{bmatrix} -I[i \times i] & 0[i \times j] & C_p^v[i \times k] & -C_p^v[i \times k] \\ 0[j \times i] & -I[j \times j] & C_p^x[j \times k] & -C_p^x[j \times k] \end{bmatrix} \quad (21)$$

$$u = \begin{bmatrix} F_i[i \times 1] \\ M_j[j \times 1] \\ E_k^U[k \times 1] \\ E_k^D[k \times 1] \end{bmatrix} \quad (22)$$

$$\begin{cases} F_i = \ln\left(\frac{v_i}{v_{i,ref}}\right) \\ M_j = \ln\left(\frac{x_j}{x_{j,ref}}\right) \\ E_k = \ln\left(\frac{p_k}{p_{k,ref}}\right) \end{cases} \quad (23)$$

$$\tilde{F}_i = F_i + \ln(v_{i,ref}) \quad (24)$$

$$\tilde{M}_j = M_j + \ln(x_{j,ref}) \quad (25)$$

Table 2. Indices, variables, and parameters used in the NRA formulation.

Index letter	Type	Refers to	Set or unit
i	Index	Reaction	$i \in \mathcal{I}$
j	Index	Metabolite	$j \in \mathcal{J}$
k	Index	Enzyme	$k \in \mathcal{K}$
m	Index	Metabolite participating in reaction i	$m \in \mathcal{M}$
v_i	Variable	Flux of reaction i	$mmol \cdot gDW^{-1} \cdot h^{-1}$
x_j	Variable	Concentration of metabolite j	M
p_k	Variable	Catalytic activity of enzyme k	$mmol \cdot h^{-1}$
\tilde{F}_i	Variable	Scaled flux deviation of reaction i	$\tilde{F}_i \in \mathbb{R}$
F_i	Variable	Flux deviation of reaction i	$F_i \in \mathbb{R} \cap [lb_F, ub_F]$
\tilde{M}_j	Variable	Scaled concentration deviation of metabolite j	$\tilde{M}_j \in \mathbb{R}$
M_j	Variable	Concentration deviation of metabolite j	$M_j \in \mathbb{R} \cap [lb_M, ub_M]$
E_k	Variable	Catalytic activity deviation of enzyme k	$E_k \in \mathbb{R} \cap [lb_E, ub_E]$
E_k^U	Variable	Upregulation of catalytic activity of enzyme k	$E_k^U \in \mathbb{R} \cap [0, ub_E]$
E_k^D	Variable	Downregulation of catalytic activity of enzyme k	$E_k^D \in \mathbb{R} \cap [0, -lb_E]$
$\Delta_r G'_i$	Variable	Gibbs free energy change of reaction i	$\Delta_r G'_i \in \mathbb{R}$
$\Delta_r G'^o_i$	Variable	Standard Gibbs free energy change of reaction i	$\Delta_r G'^o_i \in \mathbb{R} \cap [\Delta_r G'^o_{i,est} \pm err]$
u	Variable	Vector of NRA variables	$u \in \mathbb{R}^{(\mathcal{J}+\mathcal{J}+2\mathcal{K})}$
E_k^{UU}	Variable	Binary upregulation of catalytic activity of enzyme k	$E_k^{UU} \in \{0,1\}$
E_k^{DU}	Variable	Binary downregulation of catalytic activity of enzyme k	$E_k^{DU} \in \{0,1\}$
z_k	Variable	Deregulation of enzyme k	$z_k \in \{0,1\}$
C_p^v	Parameter	Flux control coefficient	$C_p^v \in \mathbb{R}$
C_p^x	Parameter	Concentration control coefficient	$C_p^x \in \mathbb{R}$
$v_{i,ref}$	Parameter	Reference flux of reaction i	$mmol \cdot gDW^{-1} \cdot h^{-1}$
$x_{j,ref}$	Parameter	Reference concentration of metabolite j	M
$p_{k,ref}$	Parameter	Reference catalytic activity of enzyme k	$mmol \cdot h^{-1}$
N	Parameter	Stoichiometric matrix	$N \in \mathbb{R}^{\mathcal{J} \times \mathcal{J}}$
K	Parameter	NRA matrix	$K \in \mathbb{R}^{(\mathcal{J}+\mathcal{J}) \times (\mathcal{J}+\mathcal{J}+2\mathcal{K})}$
lb_F	Parameter	Flux deviation lower bound	$lb_F \in \mathbb{R}$
ub_F	Parameter	Flux deviation upper bound	$ub_F \in \mathbb{R}$
lb_M	Parameter	Concentration deviation lower bound	$lb_M \in \mathbb{R}$
ub_M	Parameter	Concentration deviation upper bound	$ub_M \in \mathbb{R}$
lb_E	Parameter	Catalytic activity deviation lower bound	$lb_E \in \mathbb{R}$
ub_E	Parameter	Catalytic activity deviation upper bound	$ub_E \in \mathbb{R}$
$\Delta_r G'^o_{i,est}$	Parameter	Estimated standard Gibbs free energy change of reaction i	$\Delta_r G'^o_{i,est} \in \mathbb{R}$
err	Parameter	Associated error on the estimated standard Gibbs free energy change of reaction i	$err \in \mathbb{R}$
R	Parameter	Gas constant	$R = 1.9872 \times 10^{-3} kcal \cdot K^{-1} \cdot mol^{-1}$
T	Parameter	Temperature	K
ξ	Parameter	User-defined large constant	$\xi \in \mathbb{N} : \xi > max\{ ub_E , lb_E \}$
α_0	Parameter	Minimum user-defined productivity	$mmol \cdot gDW^{-1} \cdot h^{-1}$
α_1	Parameter	Minimum user-defined yield	$\alpha_1 \in \mathbb{R}$
α_2	Parameter	Minimum user-defined growth rate	h^{-1}

α_3	Parameter	Maximum user-defined O_2 requirement	$mmol \cdot gDW^{-1} \cdot h^{-1}$
β_0	Parameter	Minimum user-defined productivity	$\beta_0 \in \mathbb{R} \cap [lb_F, ub_F]$
β_1	Parameter	Minimum user-defined yield	$\beta_1 \in \mathbb{R}$
β_2	Parameter	Minimum user-defined growth rate	$\beta_2 \in \mathbb{R} \cap [lb_F, ub_F]$
β_3	Parameter	Maximum user-defined number of interventions	$\beta_3 \in \mathbb{N}$
β_4	Parameter	Maximum user-defined O_2 requirement	$\beta_4 \in \mathbb{R} \cap [lb_F, ub_F]$

140

141 Importantly, the NRA formulation allows us to prevent thermodynamically infeasible designs
142 because it naturally includes thermodynamic constraints regarding the Gibbs free energy
143 change ($\Delta_r G'_i$) of each reaction (eq. 15). Furthermore, the proposed formulation allows
144 imposing additional design criteria such as production robustness and operational
145 parameters (Eqs. 16-19). The NRA optimization problems can be solved with the TFA toolbox
146 (Salvy et al., 2019). We provide more details about the NRA formulation in Methods.

147

148 **Strain design with physiological and design constraints for improved glucose uptake**

149 Metabolic engineering interventions on pathways inevitably result in altered reaction rates
150 as well as metabolite concentration levels. NRA, being a constraint-based method, allows for
151 setting appropriate constraints on these quantities. Both fluxes and concentrations need to
152 be constrained within realistic physiological bounds, conditional to each case study. For
153 instance, severe changes in metabolic concentrations upon metabolic engineering
154 interventions could significantly influence the organism's growth or even lead to an excess of
155 toxic byproducts. The strain design should likewise consider that enzyme expression levels
156 cannot increase beyond the currently reported experimentally achievable levels, and it
157 cannot allow an infinite increase of reaction fluxes in the network. In contrast, the design
158 should also be able to model gene knockouts by allowing both enzyme activities and reaction
159 fluxes to decrease close to zero.

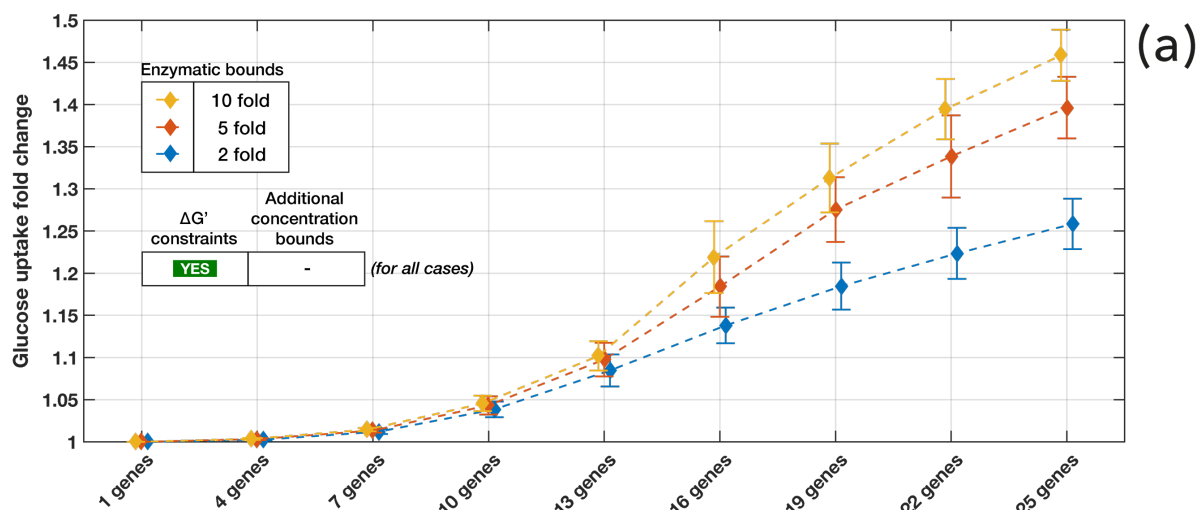
160 Here, we examined the effects of the imposed physiological and design constraints on the
161 strain design for improved glucose uptake. To this end, we analyzed the achievable glucose
162 uptake rates with 2-fold, 5-fold, and 10-fold maximum allowable deviation of enzyme
163 activities from the reference level for a set of designs ranging from 1 to 25 gene manipulations
164 (Figure 2a). The metabolite concentrations were subject to the thermodynamic feasibility
165 constraints (Methods), and within the predefined physiological ranges (10nM - 0.1M) for each
166 cellular compartment. We allowed the fluxes to increase up to 10-fold of their reference level,

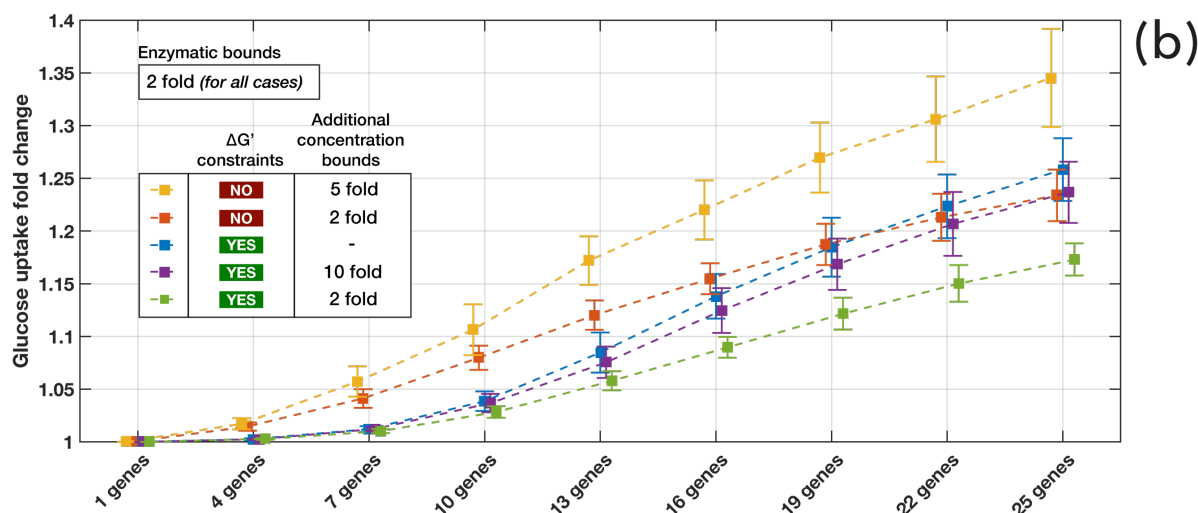
167 and both fluxes and enzyme activities could reduce to zero. The latter means that solutions
168 can include potential gene knockouts. As a mean to investigate the sensitivity of obtained
169 solutions, we repeated the study for one reference and 18 extreme sets of control coefficients
170 (Methods).

171 As the allowable enzyme activity change (Eqs. 10 and 23) increased from 2- to 10-fold, the
172 predicted attainable glucose uptake rate was about the same for up to 10 gene
173 manipulations, indicating that for a small number of gene manipulations the upper limits on
174 enzyme activity were not a limiting factor (Figure 2a). However, starting from 13 gene
175 manipulations, the difference between the predictions increased considerably. As expected,
176 the higher limits on enzyme activity, the larger predicted improvement of glucose uptake was
177 observed. For example, NRA predicted for 25 gene manipulations that glucose uptake rate
178 would increase by 26%, 39%, and 46% for 2-, 5-, and 10-fold change in enzyme activity,
179 respectively. Interestingly, the predicted fold change of the glucose uptake across the
180 nineteen studied reference and extreme CC-sets varied similarly for the designs with 13 or
181 more gene manipulations (Figure 2a whiskers). This rather constant variability as we go
182 toward a higher number of gene manipulations suggests that variability among 19 sets is
183 primarily determined by the activity of a relatively small number of enzymes, which
184 predominantly have control over the glucose uptake rate. This finding is in line with previous
185 studies of metabolic systems demonstrating that just a few enzymes in the network (or
186 corresponding parameters) determine the key metabolic properties such as system stability
187 (Andreozzi et al., 2016b) or control over production fluxes (Miskovic et al., 2019a). A similar
188 observation was reported in a more general context of biological systems (Daniels et al., 2008;
189 Gutenkunst et al., 2007).

190 Next, we investigated how constraints on concentration deviations (Eqs. 9 and 23) affect the
191 attainable glucose uptake. This is a salient aspect of strain design because metabolic
192 engineers have to ensure that metabolite concentrations remain within physiological bounds.
193 For instance, it is vital not to exceed toxicity levels for some compounds. The studies on the
194 effects of metabolite concentration constraints have also to consider thermodynamics
195 because it is well known that the standard free Gibbs energy change of reactions couples the
196 reaction directionalities and the metabolite concentrations (Ataman and Hatzimanikatis,
197 2015). For this analysis, we have performed several studies by imposing different

198 concentration bounds together with and without thermodynamic constraints (Figure 2b). In
199 general, our results suggest that NRA without thermodynamic constraints tends to
200 overpredict the increase in glucose uptake (Figure 2b), meaning that thermodynamic
201 constraints are limiting factors of strain design. The notable exception was that, starting from
202 19 gene manipulations, the 2-fold constraints on concentrations are more limiting than the
203 thermodynamic ones (Figure 2b blue & orange lines). As expected, our results also show that
204 the tighter the concentration deviation bounds we impose, the less important improvements
205 of glucose uptake could be attained (Figure 2b). For example, the attainable increase of
206 glucose uptake rate with the thermodynamic and additional 2-fold and 10-fold constraints for
207 25 gene manipulations were 17% and 24%, respectively (Figure 2b, green and violet). We also
208 observed that the variance of glucose uptake increase was smaller as the concentration
209 bounds became more constrained. Similarly, we observed a trend that the variance in the
210 studies with the thermodynamic constraints was smaller than in the ones without
211 thermodynamic constraints.





213

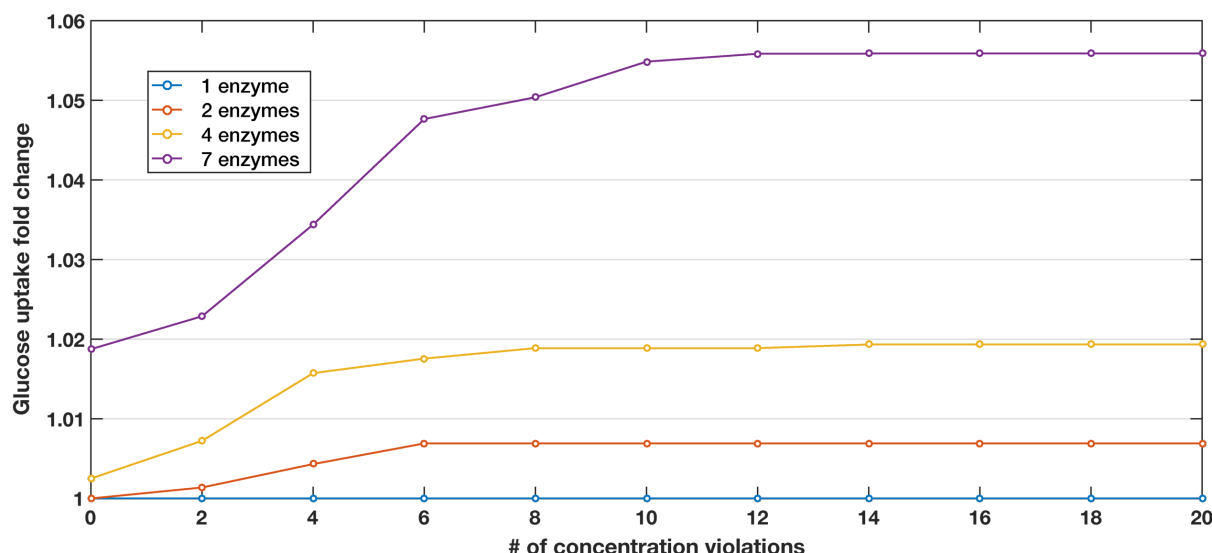
214 *Figure 2. Effects of the physiological and design constraints on glucose uptake rate for a set of designs*
215 *with different number of gene manipulations. Effects of: (a) allowed 2-fold (blue), 5-fold (orange), and*
216 *10-fold (yellow) changes in enzyme perturbation magnitude, and (b) different imposed metabolite*
217 *concentration bounds. The study was performed for one reference and 18 extreme sets of CCs selected*
218 *using PCA (Methods). In all cases, the fluxes were allowed to increase 10-fold and decrease to zero.*
219 *The whiskers and the respective symbols indicate the interquartile ranges and the means of the*
220 *considered CC-sets, respectively, as adjusted by the Bonferroni correction (Methods). Blue lines*
221 *correspond in both graphs.*

222

223 Metabolite concentrations limiting the glucose uptake

224 Having demonstrated that limits on metabolite concentrations, either thermodynamic
225 constraints or physiological limitations, significantly affect the attainable glucose uptake, we
226 investigated how many and which metabolite concentrations should violate the
227 thermodynamic constraints to achieve a higher glucose uptake. For simplicity and clarity of
228 exposition, we allowed designs with one, two, four, and seven gene manipulations (Figure 3).

229 In the cases of one and two gene manipulations, the flux through glucose uptake could not
230 be modified with the thermodynamically feasible concentrations (zero violations). For a larger
231 number of gene manipulations, a small increase in glucose uptake could be achieved even
232 without violating the thermodynamics. For example, the manipulation of seven genes would
233 yield ~2% of glucose uptake increase for zero violations. However, when we allowed some
234 concentration deviations to exceed their bounds, the potential violations pushed the
235 attainable glucose uptake to higher values (Figure 3). For instance, the seven gene
236 manipulations design with ten concentration violations would result in 5.5% increase in
237 glucose uptake.



238

239 *Figure 3. Maximal attainable increase in glucose uptake as a function of a different number of*
240 *metabolite concentration violations for one, two, four, and seven gene modifications. The fluxes were*
241 *allowed to increase 10-fold and decrease to zero, the non-violated concentration bounds were subject*
242 *to the thermodynamic constraints, and the enzymatic bounds were set to 2-fold. The reference model*
243 *was used for all cases.*

244 Next, we focused on finding which were the metabolites whose concentration constraints
245 should be violated to improve glucose uptake. To this end, we studied the case of four
246 violations and two, four, and seven gene manipulations. For each gene manipulation study,
247 we obtained the unique sets of four metabolite concentrations violating constraints (Table
248 3a). The three gene manipulation studies involved, in total, seven species with concentrations
249 violating the thermodynamic constraints. Among the seven species, peroxisomal protons
250 appeared in all three studies. Moreover, irrespectively of the study, to achieve a higher
251 glucose uptake, the concentrations of protons (both cytosolic and peroxisomal), AMP, and
252 phenylalanine needed to be increased, while the ones for CTP, dCTP and glutamine needed
253 to be decreased. The violations ranged from 2% for the case of cytosolic hydrogen to 57% for
254 the case of CTP (Supplementary Table S1).

255 This analysis provides an opportunity to focus on each of the identified molecules, draw
256 hypothesis about their role in the system limitations, and investigate these interplays and
257 ways to overcome them *in vitro*. For example, it suggested that the pH value in compartments
258 can be a limiting factor for metabolic design.

259

260 *Table 3. Sets of four metabolite species with concentrations violating thermodynamic constraints for*
261 *designs with two, four, and seven gene manipulations. The arrows indicate should a metabolite*
262 *concentration be increased or decreased to improve glucose uptake. c: cytosol, p: periplasm.*

Metabolite concentrations	# of parameter manipulations		
	2	4	7
AMP (c) ↑	X	-	X
CTP (c) ↓	-	X	X
dCTP (c) ↓	-	X	-
H ⁺ (c) ↑	X	X	-
H ⁺ (p) ↑	X	X	X
L-Glutamine (c) ↓	-	-	X
L-Phenylalanine (c) ↑	X	-	-

263

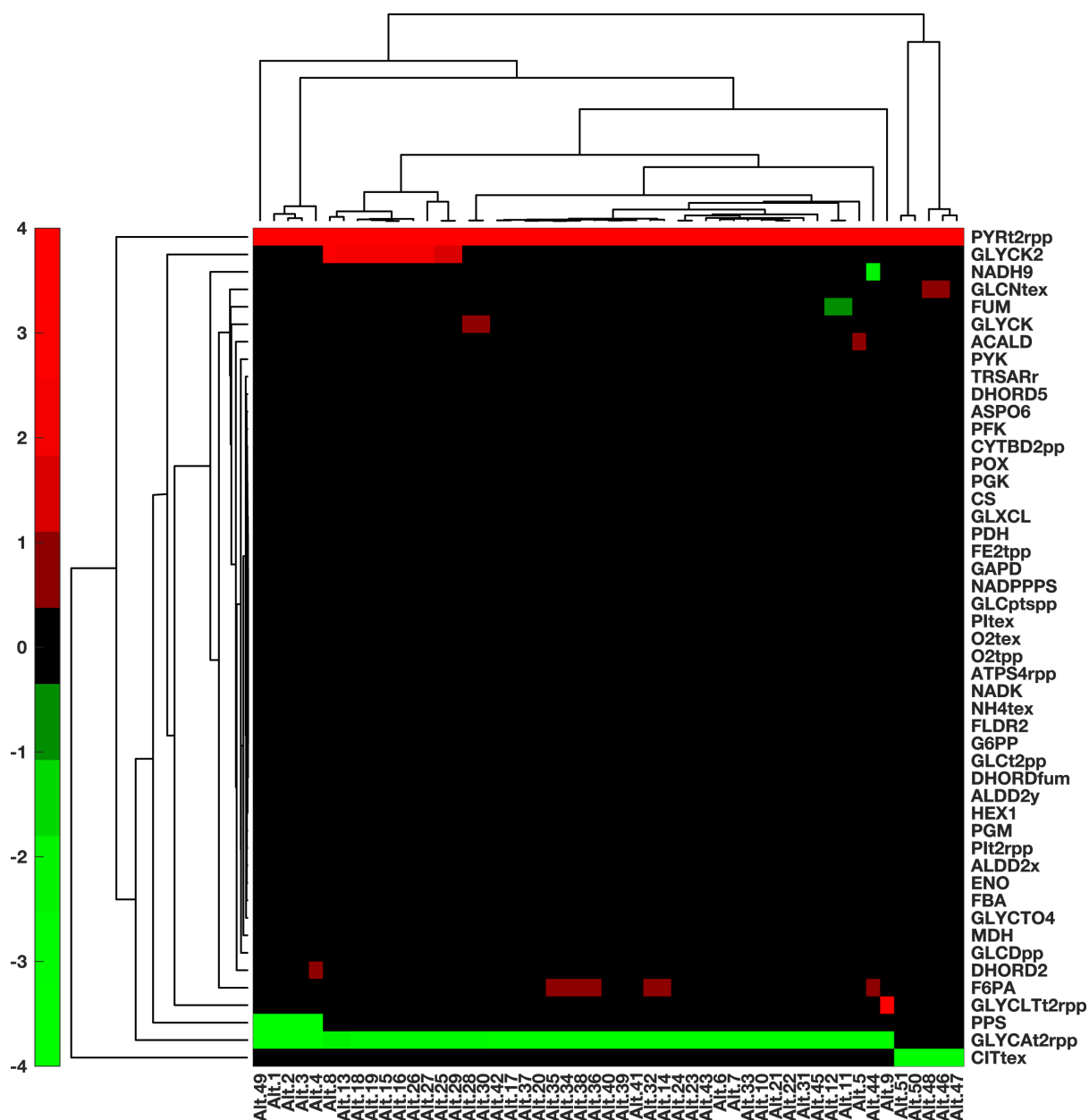
264 **NRA design for Pyruvate production considers together specific production rate and yield**

265 Pyruvate (pyruvic acid) is widely used in the food, chemical, and pharmaceutical industries. It
266 is a precursor for the synthesis of various amino acids, and has been used for the production
267 of antioxidants, food additives and supplements, pharmaceutical precursors, and biofuels
268 (Atsumi et al., 2008; Kalman et al., 1999; Li et al., 2001; Zhang et al., 2010). The microbial
269 production of pyruvate has been largely explored, and has involved both strain and process
270 engineering and development (Maleki and Eiteman, 2017). In *E. coli*, pyruvate has been
271 identified as one of the main hubs for the production of non-native commercial products
272 (Zhang et al., 2016). The most common approach in microbial engineering for the
273 overproduction of pyruvate is through deletions of the downstream utilization of pyruvate
274 towards byproducts such as acetate, acetyl-CoA, and ethanol among others (Akita et al., 2016;
275 Causey et al., 2004; Zhu et al., 2008).

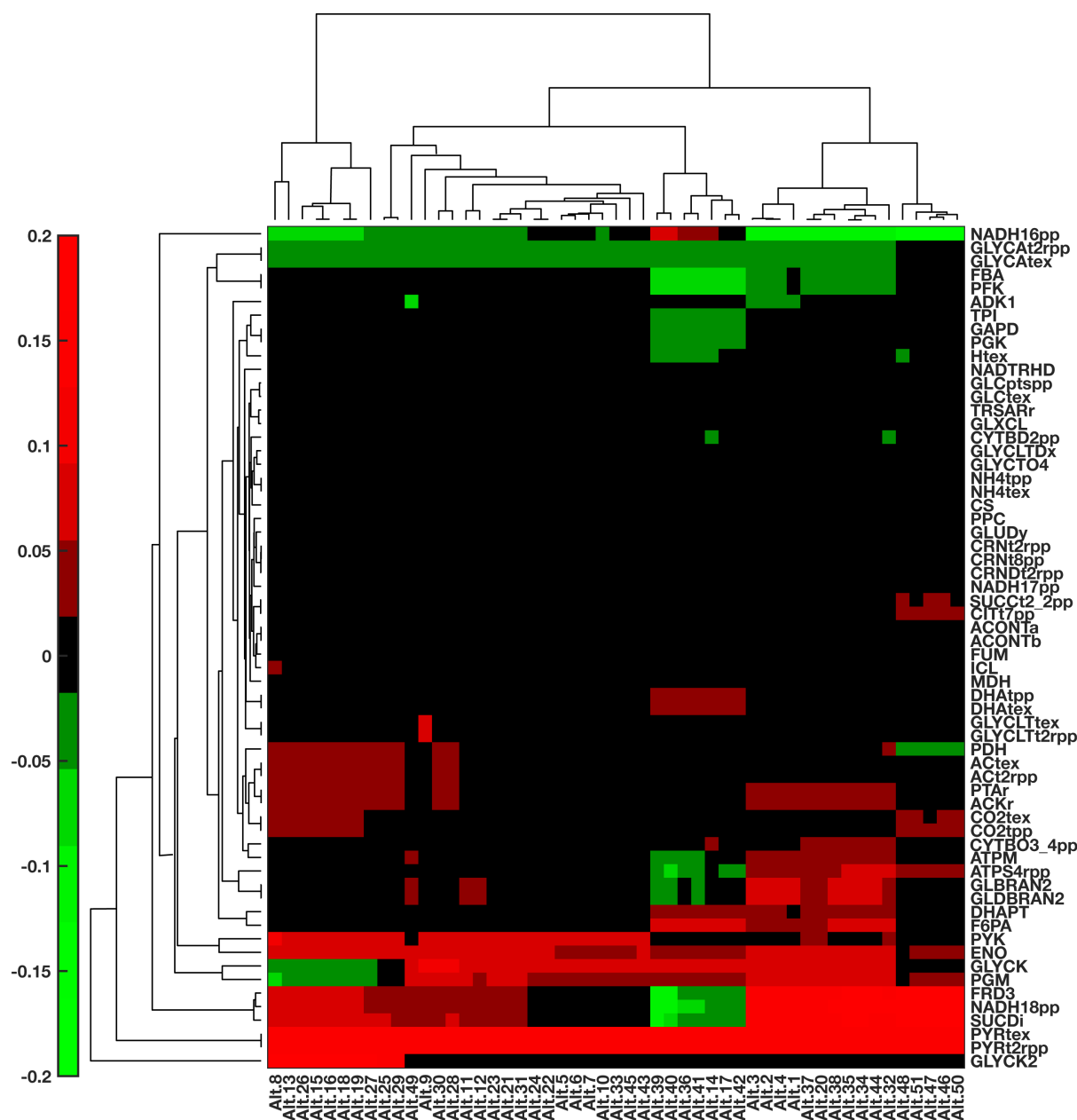
276 To illustrate the features and flexibility of the NRA method, we showcase design for the
277 improved specific productivity rate of pyruvate while taking into account the yield of pyruvate
278 from glucose, design constraints, and thermodynamic feasibility. We imposed the following
279 design and physiology constraints: (i) up to five gene/enzyme activity manipulations, (ii) the
280 genes encoding for metabolic enzymes could either be upregulated up to 50-fold or

281 downregulated down to a knockout, (iii) the fluxes could increase up to 100-fold for
282 upregulation and decrease down to zero for knockouts, and (iv) the concentration values
283 were subject to the thermodynamic feasibility constraints and the physiological ranges (10nM
284 - 0.1M). Given these constraints, we first performed an optimization to determine the
285 maximum yield of pyruvate from glucose. Then, we added the pyruvate yield to be at least
286 90% of this value to the set of constraints and maximized the specific pyruvate productivity
287 rate. In this manner, we were able to implicitly account for the potential tradeoffs of yield
288 and productivity that can occur in such designs.

289 We generated 51 alternative designs with five gene manipulations providing at least 99% of
290 the maximum specific productivity rate of pyruvate and fulfilling the imposed constraints. The
291 alternative designs involved the manipulation of genes corresponding to 48 distinct enzymes
292 (Supplementary Table S2). All cases provided over a 22-fold increase in both the pyruvate
293 yield and specific productivity rate compared to the reference state. To understand better
294 the mechanisms and identify metabolic patterns behind improved pyruvate production and
295 yield, we performed clustering analysis over 51 designs with respect to (i) the 48 enzyme
296 activity manipulations (Figure 4), and (ii) predicted change in metabolic fluxes upon changes
297 in enzyme activities (Figure 5). For the clustering based on the absolute change in fluxes, we
298 used the set of 67 reactions that had an absolute flux change of more than 0.01 mmol/gDW/h.
299 The transport of pyruvate from the cytosol to the periplasm (PYRt2rpp) appeared as a target
300 in all designs with 50-fold upregulation of the PYRt2rpp encoding gene (Figure 4). The
301 upregulation of glycolytic enzymes and enzymes leading to pyruvate synthesis would also
302 improve pyruvate production, with the most prominent target being glycerate kinase
303 (GLYCK2). We also observed knockouts (or significant downregulations) with the majority of
304 downregulated genes involving the consumption of pyruvate towards the formation of
305 byproducts. Among these, the periplasmic transport of glycerate (GLYCAt2rpp) was present
306 in most generated sets, being replaced by the extracellular transport of citrate (CITtex) in a
307 few cases (Figure 4). We also observed the knockout of PPS (Phosphoenolpyruvate synthase),
308 which is associated with the conversion of pyruvate to phosphoenolpyruvate.



320 (Supplementary Table S2); (iv) a knockout of PPS for alternatives 1-4, 49 or a slight
321 downregulation of fructose-bisphosphate aldolase (FBA) for alternatives 20, 32, 34, 35, 37,
322 38, and 44.



323
324 *Figure 5. Hierarchical clustering of the 51 alternative designs for the increase of pyruvate productivity,*
325 *based on the absolute change in flux value of the 67 most affected reactions in the network.*

326
327 As a result of these manipulations, the carbon flow was re-directed from the secretion of (R)-
328 glycerate toward the production of phosphoenolpyruvate through glycerate kinase (GLYCK),
329 phosphoglycerate mutase (PGM), and ENO (Figure 6 and Supplementary Figure S1).
330 Downstream, phosphoenolpyruvate is converted to pyruvate through dihydroxyacetone

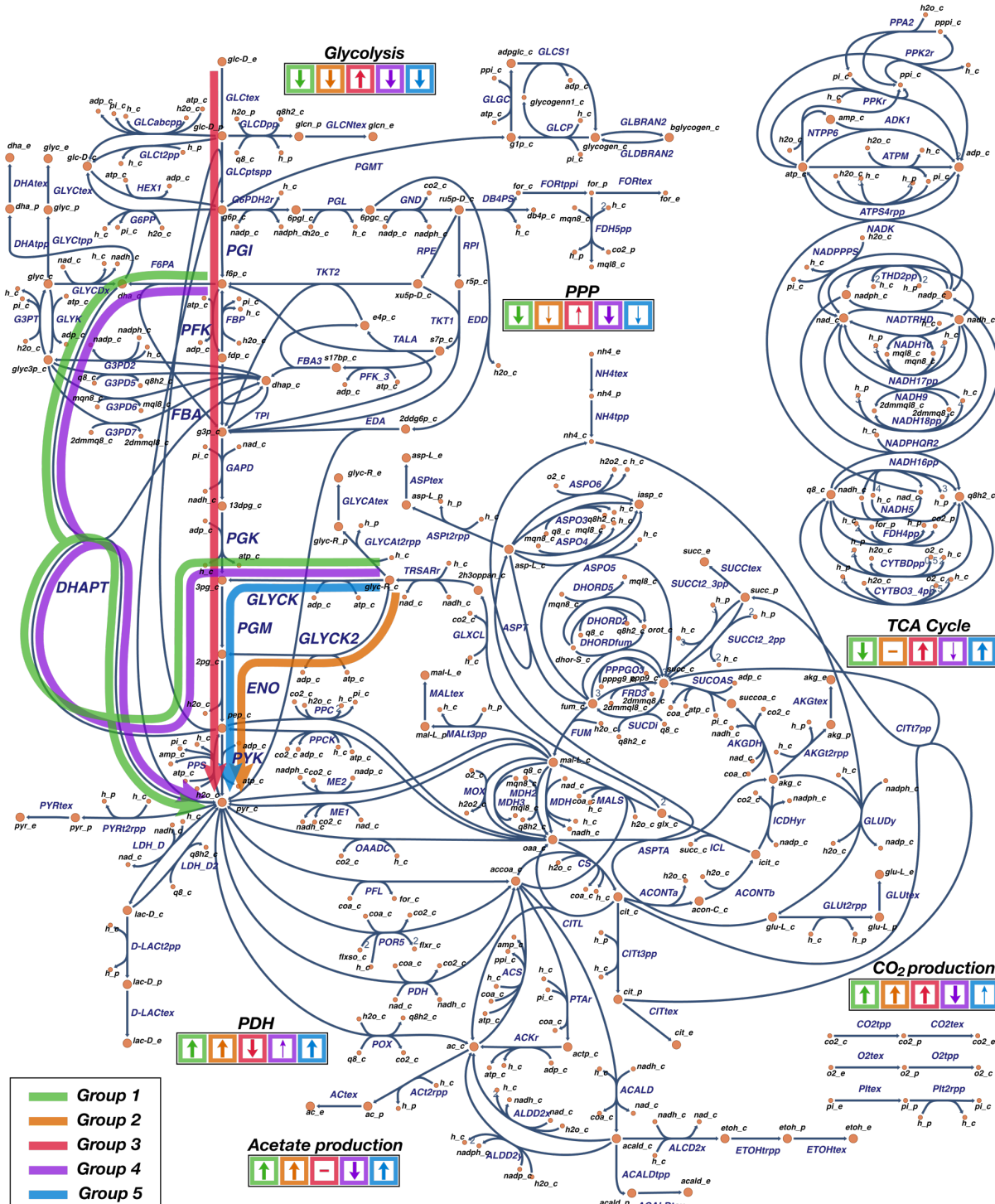
331 phosphotransferase (DHAPT), whose activity was also increased. This group is further
332 characterized by a slight increase in acetate production and CO₂ secretion, and a deregulation
333 of the ATP metabolism such as an increase of the ATP non-growth associated maintenance
334 (ATPM) or a decrease in activity of adenylate kinase (ADK1) for alternatives 1-4, 49. Moreover,
335 the conversion of fructose-6-phosphate to glyceraldehyde-3-phosphate instead through FBA
336 and phosphofructokinase (PFK) was diverted through F6PA.

337 The second group consisting of alternatives 8, 13, 15, 16, 18, 19, 25-27, and 29 shared the
338 manipulations (i) and (ii) with the first group. In addition, this group involved: (iii) an
339 upregulation of glycerate kinase GLYCK2; and (iv) a slight upregulation of pyruvate kinase
340 (PYK). The observed effects of these manipulations were similar to the ones of the first group
341 with the increased activity of lower glycolysis and acetate secretion pathway (Figures 5, 6 and
342 Supplementary figure S2). The notable difference was that the carbon diverted from glycerate
343 secretion was channeled through GLYCK2, ENO, and PYK to pyruvate. Furthermore, we
344 observed a slight increase in activity of the TCA cycle and pyruvate dehydrogenase (PDH),
345 whereas the ATP metabolism remained mostly unchanged.

346 The third group formed by alternatives 46-48, 50, and 51 was distinct from the other groups
347 because it involved strategy to knockout citrate transport CITtex instead of GLYCA₂rpp
348 (Figure 4). Additional manipulations in these group were a slight downregulation of citrate
349 synthase (CS) and a slight upregulation of glycolytic enzymes PGM (Alternatives 46, 47, 50,
350 51) or ENO (Alternative 48). Overall, these manipulations resulted in increased activity of the
351 upper and lower glycolysis, pentose phosphate pathway, and the TCA cycle (Figure 6 and
352 Supplementary Figure S3). This was the only group with increased activity of the upper
353 glycolysis. We have also observed a decrease in activity of PDH (Figures 5 and Supplementary
354 Figure S3).

355 The fourth group constituted by alternatives 14, 17, 36, 39-42 had a distinct pattern in the
356 network flux distributions while sharing manipulations (i)-(iii) with the first group (Figure 5, 6
357 and Supplementary Figure S4). A slight downregulation of PFK together with manipulations
358 (i)-(iii) had a considerable impact by reducing the activity of the reactions in the upper
359 glycolysis (PFK, FBA, triose-phosphate isomerase (TPI), glyceraldehyde-3-phosphate
360 dehydrogenase (GAPD), phosphoglycerate kinase(PGK)), the ETC chain (NADH dehydrogenase
361 (NADH18pp), Cytochrome oxidase bo3 (CYTBO3_4pp) and the ATP metabolism (ATPM and

362 ATP synthase (ATPS4rpp)). We have also observed, in contrast to other groups, a reduced
 363 activity in CO₂ and acetate secretion pathways.



364
 365 Figure 6. Overview of metabolic engineering strategies devised using NRA for the improved specific
 366 production rate of pyruvate while preserving the prespecified yield of pyruvate from glucose. 51
 367 strategies devised with NRA were categorized in 5 distinct groups. The thick arrows on the graph
 368 denote the principal ways of carbon re-direction from the wild-type strain steady-state fluxes. The
 369 arrows in the colored boxes denote if the activity of the corresponding metabolic subsystem
 370 (glycolysis, pentose phosphate pathway (PPP), TCA cycle, acetate production, and CO₂ production) or

371 reaction (PDH) was increased (arrow up), decreased (arrow down), or remained unchanged (dash).
372 The thicker arrow in the colored boxes, the higher change in the activity occurred.

373
374 The fifth group, composed of alternatives 5-7, 9-12, 21-24, 28, 30, 31, 33, 43, 45, and the
375 second group have in common manipulations (i), (ii), and (iv) (Figure 4 and Supplementary
376 Table S2). Additionally, the fifth group involved either a very slight upregulation of glycolytic
377 enzymes PGM, ENO, and PGK (alternatives 11, 12, 21-24, 31, 43, and 45) or a very slight
378 downregulation of PDH (alternatives 5-7, 10, 28, and 30). As expected, the resulting flux
379 distribution was similar to the one of the second group (Supplementary Figure S5). The
380 difference was that in this group the carbon from (R)-glycerate was diverted to 2-
381 phosphoglycolate through GLYCK and PGM instead through GLYCK2 as it was done in the
382 second group. Overall, compared to other groups, the manipulations of this group have
383 changed the least the network flux distribution (Figure 5).

384 Once the principal strategies are determined, the final decision is made by experts based on
385 the comparative analysis of the proposed alternative groups and on considerations about the
386 practical implementation of the designs.

387
388 *Comparison with targets determined by looking only at unconstrained specific productivity*

389 We proceeded by examining how different are the targets obtained with the NRA design from
390 the ones determined by looking only the specific productivity rate of pyruvate. This
391 comparison will reveal how the physiology and design constraints affect our design decisions.
392 To this end, we computed the mean values of the control coefficient of the specific
393 productivity rate of pyruvate with respect to network enzyme activities, and then ranked
394 them according to their absolute value. Most of the top 15 enzymes represent either
395 extracellular transports such as oxygen uptake and ammonium secretion, as well as glycolysis
396 reactions leading to the synthesis of pyruvate (Table 4). Interestingly, the majority of these
397 enzymes do not appear as targets in any of the NRA alternatives (Table 4 and Supplementary
398 Table S2). Some of these enzymes exhibit a large control over multiple fluxes and
399 concentrations across the metabolic network. These are, therefore, severely constrained by
400 the imposed specifications in the constrained NRA design. This suggests that the NRA
401 formulation will favor parameters that have less control over the network, ensuring that
402 cellular balance will not be excessively perturbed.

403

404 *Table 4. Top ranked parameters based on their control over pyruvate production flux PYRtex. Ranking*
405 *was computed based on the mean values of 50'000 sets of Control Coefficients.*

Rank	Parameter Name	Control over PYRtex
1	NH4tex	negative
2	O2tpp	negative
3	NH4tpp	negative
4	ATPS4rpp	positive
5	GLCtex	positive
6	O2tex	negative
7	TPI	positive
8	PGI	positive
9	PFK	positive
10	RPI	negative
11	PItex	positive
12	PGM	positive
13	GLCptspp	positive
14	RPE	positive
15	PYRt2rpp	positive

406

407 Materials and Methods

408 Metabolic Control Analysis notions

409 In MCA, the CCCs, C_p^x , and the FCCs, C_p^v , are defined as the fractional change of metabolite
410 concentrations x and metabolic fluxes v , respectively, in response to a fractional change of
411 system parameters p (Hatzimanikatis and Bailey, 1996; Kacser et al., 1995). These CCs serve
412 as measurable outputs that provide information about the levels of control that system
413 parameters have on the studied biological system and physiology. From the log(linear)
414 formalism (Hatzimanikatis et al., 1996a; Reder, 1988), C_p^x and C_p^v can be derived through the
415 following expressions:

$$416 \quad C_p^x = -(NVE)^{-1} N V \Pi$$

$$417 \quad C_p^v = E C_p^x + \Pi$$

418

419 where N is the stoichiometric matrix, V is the diagonal matrix whose elements are the steady-
420 state fluxes, E is the elasticity matrix with respect to metabolites and Π is the matrix of
421 elasticities with respect to parameters.

422 Hence, flux and concentration control coefficients are computed for each reaction flux i and
423 metabolite concentration j with respect to the system parameter k as:

424

$$C_{p_k}^{v_i} = \frac{d \ln v_i}{d \ln p_k} = \frac{p_k}{v_i} \frac{d v_i}{d p_k}$$

425

$$C_{p_k}^{x_j} = \frac{d \ln x_j}{d \ln p_k} = \frac{p_k}{x_j} \frac{d x_j}{d p_k}$$

426

427 **Model description and calculation of control coefficients**

428 The stoichiometric model that was used in this study (Hameri et al., 2019c) was systematically
429 reduced from the *E. coli* iJO1366 genome-scale model (Orth et al., 2011) around the originally
430 defined reaction subsystems of glycolysis, pentose phosphate pathway (PPP), tricarboxylic
431 acid (TCA) cycle, glyoxylate cycle, pyruvate metabolism and the electron transport chain
432 (ETC), and describes the aerobically grown physiology of *E. coli* (Supplementary Table S3). The
433 reduction was performed through the redGEM and the lumpGEM algorithms (Ataman et al.,
434 2017; Ataman and Hatzimanikatis, 2017), thus ensuring preservation of as much information
435 as possible as well as that thermodynamic feasibility constraints are respected. This model
436 constitutes of 337 metabolites participating in 647 reactions, which are in turn associated
437 with 271 enzymes that serve as parameters in the NRA formulation. The model was curated
438 with thermodynamic feasibility constraints using TFA (Henry et al., 2007; Salvy et al., 2019)
439 and relevant fluxomics data (McCloskey et al., 2014). The representative steady state profiles
440 of the metabolite concentrations and metabolic fluxes were chosen with Principal
441 Component Analysis (PCA) as detailed in (Hameri et al., 2019b). Then, the populations of
442 control coefficients were built using the ORACLE workflow (Andreozzi et al., 2016a; Miskovic
443 et al., 2017; Miskovic and Hatzimanikatis, 2010; Tokic et al., 2020).

444 The CCs of the analyzed quantities (glycose uptake, pyruvate production, yield of pyruvate
445 from glucose) with respect to the lumped reactions, exchange reactions, individual biomass

446 building block contributions, and moieties were not considered in any study (Supplementary
447 Table S3).

448

449 **Addressing variability in control coefficients**

450 A common issue in MCA and in kinetic modeling is the uncertainty stemming from the scarcity
451 of knowledge concerning the kinetic properties of enzymes (Miskovic and Hatzimanikatis,
452 2011; Miskovic et al., 2015; Miskovic et al., 2019b; Wang et al., 2004). The usual approach in
453 addressing this issue involves the generation of a population of the CCs, and statistical analysis
454 thereof. To form the NRA models, we need to select sets of CCs that will be representative of
455 the generated population.

456 To select a representative set of CCs for our analysis, we took the population of 50'000 sets
457 of FCCs and CCCs computed with ORACLE for the aerobically grown *E. coli* in (Hameri et al.,
458 2019c). We first identified the vector of FCCs that was closest to the mean of the FCC
459 distribution with respect to glucose uptake and selected it as the representative set. Four
460 glucose uptake reactions in the model of *E. coli* exist with GLCptspp being responsible for
461 91.21% of the total flux through these reactions. We enforced this ratio in all performed NRA
462 studies.

463 Since the model is constrained to grow on minimal media with glucose as its sole carbon
464 source, the choice of the representative set will have a strong impact on the design criteria
465 we wish to explore. To investigate the variability in results that this choice can induce, we
466 additionally selected several “extreme” CC-sets through the use of PCA. We used nine
467 principal components to describe the space of CCs with respect to glucose uptake, which lead
468 to a coverage of 96.63% of the space variance. We selected the minimum and maximum
469 corresponding CC-sets for each component (2 x 9), leading to a total of 19 sets. We then
470 constructed 19 NRA models with these CC-sets and used them in the performed studies.

471

472 **Confidence Intervals and Bonferroni correction**

473 For the computation of confidence intervals in Figure 2, we have used the Bonferroni
474 correction in order to account for the multivariate nature of our study. In univariate studies,
475 to account for the variability in samples, confidence intervals that contain the population

476 mean with the probability $1 - \alpha$ (typically, $\alpha = 5\%$) are added around each sample mean
477 (Hameri et al., 2019a). However, univariate confidence intervals cannot be used when
478 multivariate problems are studied, instead the Bonferroni's correction of confidence intervals
479 is frequently applied. In Bonferroni's correction, for a problem with p variables, to ensure the
480 level $1 - \alpha$ for all variables simultaneously, we need to choose level $1 - \alpha/p$ for each of
481 individual variables. For instance, if we want to form confidence intervals for 10 variables with
482 an overall 95% confidence level, then we need to use individual 99.5% confidence intervals.

483

484 **Thermodynamic constraints**

485 To integrate thermodynamic constraints, we assumed that reactions operate in the
486 directionality determined by the computed reference steady state. Thus, the concentrations
487 of each metabolite in the respective cellular compartment need to be such as the $\Delta_r G'_i$ of
488 each reaction remains negative. These constraints are written as a function of the standard
489 Gibbs free energy change of the reaction ($\Delta_r G'^o$) and the logarithmic concentrations of the
490 participating metabolites, as introduced by (Henry et al., 2007). The $\Delta_r G'^o$ of each reaction is
491 computed using the Group Contribution Method (Mavrovouniotis, 1990; Mavrovouniotis,
492 1991). These values are further adjusted to take into account the thermodynamic properties
493 of the relevant cellular compartments; the pH gradient and electrochemical potential for
494 transport reactions, and ionic strength of dissociated metabolites (Henry et al., 2006).

495

496 **Constraints on enzyme activities**

497 Since the activity of an enzyme in the metabolic network could either be increased or
498 decreased, but not both at the same time, we made use of integer variables in the
499 formulation. Therefore, we split the catalytic activity deviations of our system, E_k , into the
500 continuous variables E_k^U and E_k^D , which denote the upregulation and downregulation of the
501 gene encoding for enzyme k , respectively (Eqs. 11-14). As these should not have nonzero
502 values simultaneously, we define the integer binary variables E_k^{UU} and E_k^{DU} . E_k^{UU} equals one
503 if the gene catalyzing the enzyme k is upregulated and equals zero otherwise. In contrast,
504 E_k^{DU} equals zero in the case of upregulation, and it is one for downregulation. As expressed in
505 Eq. 12, only one of these variables can be active at a time, since deregulation cannot occur in
506 both directions simultaneously, or they can both be inactive for the case of no change in the

507 respective enzyme's catalytic activity. To complete the formulation, these variables are
508 further coupled to the above defined split enzymatic deviation variables through Eqs. 13 and
509 14. The integer binary variable z_k is equal to zero if the activity of enzyme k is modified in the
510 solution, and it equals to one otherwise (Eq. 11). ξ is a constant selected to be larger than the
511 absolute value of the largest enzymatic deviation constraints, lb_E and ub_E , defined in Eq. 10.

512

513 **Software and optimization parameters**

514 The computations were made on a Mac Pro workstation running Mac OS X version 10.11.6,
515 equipped with a 2.7 GHz 12-Core Intel Xeon E5 processor and 32GB DDR3 memory, using
516 MATLAB version R2016a and the IBM CPLEX solver version 12.5.1. Time limits for the solver
517 were set as following: in Figure 2(a), for 2-fold (blue line) to 10 minutes, for 5-fold (orange
518 line) to 30 minutes, and for 10-fold (yellow line) to 3 hours; in Figure 2(b), for all cases to 10
519 mins; in Figure 3, for all cases to 30 minutes; in Table 2, for all cases to 30 minutes; in the
520 pyruvate case study (Figures 4-7), for all cases 3 hours.

521

522 **Conclusions**

523 The NRA framework enables the consistent and sophisticated design of metabolic engineering
524 strategies using MCA-based control coefficients. NRA is computationally faster and simpler
525 than other approaches since the derivation of control coefficients does not require the
526 numerical integration of non-linear kinetic models, and offers the implementation of a wide
527 variety of metabolic engineering criteria. To our knowledge, this type of approach has never
528 been applied to large or genome scale kinetic models of metabolism. Using a previously
529 published large-scale kinetic model of *E. coli*, we demonstrated that the NRA formulation can
530 be applied to large-scale metabolic networks. We used the PCA method to select a number
531 of representative sets of kinetic parameters among their population, in order to effectively
532 represent the uncertainty and flexibility of the kinetic model in respect to parametrization.
533 One of the main advantages of NRA is that, being a constraint-based modeling method, it can
534 accommodate the integration of biologically relevant bounds and constraints, which ensure
535 that the proposed strategies are consistent with the entire system capabilities and limitations
536 thereof. Since the NRA model predictions can be sensitive to the user-defined bounds on the

537 allowable reaction flux, metabolite concentration and enzymatic expression deviations, the
538 importance of including relevant physiological constraints, such as thermodynamic feasibility
539 constraints, was discussed extensively. Focusing on the case of pyruvate production, a
540 compound of great industrial interest, viable metabolic engineering strategies were shown to
541 be readily derived using this formulation. Alternative solutions could also be generated and
542 evaluated on their efficiency and potential implementation. We believe that this formulation
543 will provide a refined alternative to computational genetic design, due to its simplicity and
544 modularity, and that it will continue to be enhanced through the introduction of ever-growing
545 omics data, and additional specialized constraints and objectives.

546

547 **Acknowledgements**

548 S.T. and T.H. were supported by the Swiss National Science Foundation grant
549 [315230_163423]. M.A. was supported by the RTD grant MicroscapesX within SystemsX.ch,
550 the Swiss Initiative for Systems Biology evaluated by the Swiss National Science Foundation,
551 and RobustYeast within ERA net project via SystemsX.ch. L.M. and V.H. were supported by
552 the Ecole Polytechnique Fédérale de Lausanne (EPFL).

553

554 **Supplementary Material**

555 Table S1: Metabolite concentration violation magnitudes for designs with two, four, and
556 seven gene manipulations.

557 Table S2: List of the 51 generated alternative designs with the corresponding manipulations
558 and magnitudes of manipulations, pyruvate productivity, and yield.

559 Table S3: List of aerobically grown *E.coli* model reactions, metabolites, and parameters
560 considered in the study.

561 Figure S1: Absolute differences of fluxes in the network for the Alternative 1 design (Group
562 1). Blue/pink arrows and numbers denote an up-/down-regulation of the genes encoding for
563 the respective enzyme and the corresponding fold-change value.

564 Figure S2: Absolute differences of fluxes in the network for the Alternative 25 design (Group
565 2). Blue/pink arrows and numbers denote an up-/down-regulation of the genes encoding for
566 the respective enzyme and the corresponding fold-change value.

567

568 Figure S3: Absolute differences of fluxes in the network for the Alternative 51 design (Group
569 3). Blue/pink arrows and numbers denote an up-/down-regulation of the genes encoding for
570 the respective enzyme and the corresponding fold-change value.

571 Figure S4: Absolute differences of fluxes in the network for the Alternative 40 design (Group
572 4). Blue/pink arrows and numbers denote an up-/down-regulation of the genes encoding for
573 the respective enzyme and the corresponding fold-change value.

574 Figure S5: Absolute differences of fluxes in the network for the Alternative 45 design (Group
575 5). Blue/pink arrows and numbers denote an up-/down-regulation of the genes encoding for
576 the respective enzyme and the corresponding fold-change value.

577

578 References

579 Akita, H., Nakashima, N., Hoshino, T., 2016. Pyruvate production using engineered *Escherichia*
580 *coli*. *Amb Express*. 6.

581 Andreozzi, S., Chakrabarti, A., Soh, K. C., Burgard, A., Yang, T. H., Van Dien, S., Miskovic, L.,
582 Hatzimanikatis, V., 2016a. Identification of metabolic engineering targets for the
583 enhancement of 1,4-butanediol production in recombinant *E. coli* using large-scale
584 kinetic models. *Metabolic Engineering*. 35, 148-59.

585 Andreozzi, S., Miskovic, L., Hatzimanikatis, V., 2016b. iSCHRUNK-In Silico Approach to
586 Characterization and Reduction of Uncertainty in the Kinetic Models of Genome-scale
587 Metabolic Networks. *Metabolic engineering*. 33, 158-168.

588 Ataman, M., Gardiol, D. F. H., Fengos, G., Hatzimanikatis, V., 2017. redGEM: Systematic
589 reduction and analysis of genome-scale metabolic reconstructions for development
590 of consistent core metabolic models. *Plos Comput Biol*. 13.

591 Ataman, M., Hatzimanikatis, V., 2015. Heading in the right direction: thermodynamics-based
592 network analysis and pathway engineering. *Curr Opin Biotechnol*. 36, 176-182.

593 Ataman, M., Hatzimanikatis, V., 2017. lumpGEM: Systematic generation of subnetworks and
594 elementally balanced lumped reactions for the biosynthesis of target metabolites.
595 *Plos Comput Biol*. 13, e1005513.

596 Atsumi, S., Hanai, T., Liao, J. C., 2008. Non-fermentative pathways for synthesis of branched-
597 chain higher alcohols as biofuels. *Nature*. 451, 86-U13.

598 Bailey, J. E., 1991. Toward a science of metabolic engineering. *Science*. 252, 1668-75.

599 Causey, T. B., Shanmugam, K. T., Yomano, L. P., Ingram, L. O., 2004. Engineering *Escherichia*
600 *coli* for efficient conversion of glucose to pyruvate. *Proceedings of the National
601 Academy of Sciences of the United States of America*. 101, 2235-2240.

602 Chakrabarti, A., Miskovic, L., Soh, K. C., Hatzimanikatis, V., 2013. Towards kinetic modeling of
603 genome-scale metabolic networks without sacrificing stoichiometric, thermodynamic
604 and physiological constraints. *Biotechnology journal*. 8, 1043-1057.

605 Costa, R. S., Hartmann, A., Vinga, S., 2016. Kinetic modeling of cell metabolism for microbial
606 production. *Journal of Biotechnology*. 219, 126-141.

607 Daniels, B. C., Chen, Y. J., Sethna, J. P., Gutenkunst, R. N., Myers, C. R., 2008. Sloppiness,
608 robustness, and evolvability in systems biology. *Current Opinion in Biotechnology*. 19,
609 389-395.

610 Gombert, A. K., Nielsen, J., 2000. Mathematical modelling of metabolism. *Current Opinion in
611 Biotechnology*. 11, 180-186.

612 Gutenkunst, R. N., Waterfall, J. J., Casey, F. P., Brown, K. S., Myers, C. R., Sethna, J. P., 2007.
613 Universally sloppy parameter sensitivities in systems biology models. *Plos Comput
614 Biol*. 3, 1871-1878.

615 Hadadi, N., Hatzimanikatis, V., 2015. Design of computational retrobiosynthesis tools for the
616 design of *de novo* synthetic pathways. *Curr Opin Chem Biol*. 28, 99-104.

617 Hameri, T., Boldi, M. O., Hatzimanikatis, V., 2019a. Statistical inference in ensemble modeling
618 of cellular metabolism. *PLoS Comput Biol*. 15, e1007536.

619 Hameri, T., Fengos, G., Ataman, M., Miskovic, L., Hatzimanikatis, V., 2019b. Kinetic models of
620 metabolism that consider alternative steady-state solutions of intracellular fluxes and
621 concentrations. *Metabolic Engineering*. 52, 29-41.

622 Hameri, T., Fengos, G., Hatzimanikatis, V., 2019c. The effects of model complexity and size on
623 metabolic flux distribution and control. Case study in *E. coli*. bioRxiv.
624 666859.

625 Hatzimanikatis, V., Bailey, J. E., 1996. MCA has more to say. *Journal of Theoretical Biology*.
626 182, 233-242.

627 Hatzimanikatis, V., Floudas, C. A., Bailey, J. E., 1996a. Analysis and design of metabolic
628 reaction networks via mixed-integer linear optimization. *Aiche Journal*. 42, 1277-
629 1292.

630 Hatzimanikatis, V., Floudas, C. A., Bailey, J. E., 1996b. Optimization of regulatory architectures
631 in metabolic reaction networks. *Biotechnology and Bioengineering*. 52, 485-500.

632 Henry, C., Broadbelt, L., Hatzimanikatis, V., 2007. Thermodynamics-Based Metabolic Flux
633 Analysis. *Biophysical Journal*.

634 Henry, C., Jankowski, M. D., Broadbelt, L. J., Hatzimanikatis, V., 2006. Genome-scale
635 thermodynamic analysis of *Escherichia coli* metabolism. *Biophysical Journal*. 90, 1453-
636 61.

637 Kacser, H., Burns, J. A., Fell, D. A., 1995. The Control of Flux. *Biochem Soc T*. 23, 341-366.

638 Kalman, D., Colker, C. M., Wilets, I., Roufs, J. B., Antonio, J., 1999. The effects of pyruvate
639 supplementation on body composition in overweight individuals. *Nutrition*. 15, 337-
640 340.

641 Klamt, S., Muller, S., Regensburger, G., Zanghellini, J., 2018. A mathematical framework for
642 yield (vs. rate) optimization in constraint-based modeling and applications in
643 metabolic engineering. *Metabolic Engineering*. 47, 153-169.

644 Li, Y., Chen, J., Lun, S. Y., 2001. Biotechnological production of pyruvic acid. *Appl Microbiol
645 Biot*. 57, 451-459.

646 Long, M. R., Ong, W. K., Reed, J. L., 2015. Computational methods in metabolic engineering
647 for strain design. *Current Opinion in Biotechnology*. 34, 135-141.

648 Maleki, N., Eiteman, M. A., 2017. Recent Progress in the Microbial Production of Pyruvic Acid.
649 *Fermentation-Basel*. 3.

650 Mavrovouniotis, M. L., 1990. Group Contributions for Estimating Standard Gibbs Energies of
651 Formation of Biochemical-Compounds in Aqueous-Solution. *Biotechnology and
652 Bioengineering*. 36, 1070-1082.

653 Mavrovouniotis, M. L., 1991. Estimation of Standard Gibbs Energy Changes of
654 Biotransformations. *The Journal of Biological Chemistry*. 266, 14440-14445.

655 McCloskey, D., Gangoiti, J. A., King, Z. A., Naviaux, R. K., Barshop, B. A., Palsson, B. O., Feist,
656 A. M., 2014. A model - driven quantitative metabolomics analysis of aerobic and
657 anaerobic metabolism in *E. coli* K - 12 MG1655 that is biochemically and
658 thermodynamically consistent. *Biotechnology and bioengineering*. 111, 803-815.

659 Miskovic, L., Alff-Tuomala, S., Soh, K. C., Barth, D., Salusjärvi, L., Pitkänen, J.-P., Ruohonen, L.,
660 Penttilä, M., Hatzimanikatis, V., 2017. A design-build-test cycle using modeling and
661 experiments reveals interdependencies between upper glycolysis and xylose uptake
662 in recombinant *S. cerevisiae* and improves predictive capabilities of large-scale kinetic
663 models. *Biotechnol Biofuels*. 10, 166.

664 Miskovic, L., Béal, J., Moret, M., Hatzimanikatis, V., 2019a. Uncertainty Reduction in
665 Biochemical Kinetic Models: Enforcing Desired Model Properties. *Plos Comput Biol*.
666 15, e1007242.

667 Miskovic, L., Hatzimanikatis, V., 2010. Production of biofuels and biochemicals: in need of an
668 ORACLE. *Trends in biotechnology*. 28, 391-397.

669 Miskovic, L., Hatzimanikatis, V., 2011. Modeling of uncertainties in biochemical reactions.
670 *Biotechnology and Bioengineering*. 108, 413-23.

671 Miskovic, L., Tokic, M., Fengos, G., Hatzimanikatis, V., 2015. Rites of passage: requirements
672 and standards for building kinetic models of metabolic phenotypes. *Current Opinion*
673 in *Biotechnology*. 36, 1-8.

674 Miskovic, L., Tokic, M., Savoglidis, G., Hatzimanikatis, V., 2019b. Control Theory Concepts for
675 Modeling Uncertainty in Enzyme Kinetics of Biochemical Networks. *Industrial &*
676 *Engineering Chemistry Research*. 58, 13544-13554.

677 Orth, J. D., Conrad, T. M., Na, J., Lerman, J. A., Nam, H., Feist, A. M., Palsson, B. O., 2011. A
678 comprehensive genome-scale reconstruction of *Escherichia coli* metabolism-2011.
679 *Molecular Systems Biology*. 7.

680 Orth, J. D., Thiele, I., Palsson, B. O., 2010. What is flux balance analysis? *Nat Biotechnol*. 28,
681 245-8.

682 Patil, K. R., Rocha, I., Forster, J., Nielsen, J., 2005. Evolutionary programming as a platform for
683 in silico metabolic engineering. *BMC Bioinformatics*. 6, 308.

684 Reder, C., 1988. Metabolic control theory: a structural approach. *Journal of theoretical*
685 *biology*. 135, 175-201.

686 Salvy, P., Fengos, G., Ataman, M., Pathier, T., Soh, K. C., Hatzimanikatis, V., 2019. pyTFA and
687 matTFA: a Python package and a Matlab toolbox for Thermodynamics-based Flux
688 Analysis. *Bioinformatics*. 35, 167-169.

689 Schneider, P., Klamt, S., 2019. Characterizing and ranking computed metabolic engineering
690 strategies. *Bioinformatics*. 35, 3063-3072.

691 Soh, K. S., Miskovic, L., Hatzimanikatis, V., 2012. From network models to network responses:
692 integration of thermodynamic and kinetic properties of yeast genome-scale metabolic
693 networks. *FEMS Yeast Research*. 12, 129-143.

694 Tokic, M., Hatzimanikatis, V., Miskovic, L., 2020. Large-scale kinetic metabolic models of
695 *Pseudomonas putida* KT2440 for consistent design of metabolic engineering
696 strategies. *Biotechnol Biofuels*. 13.

697 Varma, A., Boesch, B. W., Palsson, B. O., 1993. Biochemical Production Capabilities of
698 *Escherichia-Coli*. *Biotechnology and Bioengineering*. 42, 59-73.

699 Wang, L., Birol, I., Hatzimanikatis, V., 2004. Metabolic Control Analysis under Uncertainty:
700 Framework Development and Case Studies. *Biophysical Journal*. 87, 3750-3763.

701 Wang, L., Dash, S., Ng, C. Y., Maranas, C. D., 2017. A review of computational tools for design
702 and reconstruction of metabolic pathways. *Synth Syst Biotechno*. 2, 243-252.

703 Zhang, X. L., Tervo, C. J., Reed, J. L., 2016. Metabolic assessment of *E. coli* as a Biofactory for
704 commercial products. *Metabolic Engineering*. 35, 64-74.

705 Zhang, Y. N., Tao, F., Du, M. F., Ma, C. Q., Qiu, J. H., Gu, L. C., He, X. F., Xu, P., 2010. An efficient
706 method for N-acetyl-d-neuraminic acid production using coupled bacterial cells with
707 a safe temperature-induced system. *Appl Microbiol Biot*. 86, 481-489.

708 Zhu, Y. H., Eiteman, M. A., Altman, R., Altman, E., 2008. High Glycolytic Flux Improves Pyruvate
709 Production by a Metabolically Engineered *Escherichia coli* Strain. *Applied and*
710 *Environmental Microbiology*. 74, 6649-6655.

711